Copper deposition on metallic and non-metallic single particles via impact electrochemistry

Oladeji, Abiola V.; Courtney, James M.; Rees, Neil V.

DOI:
10.1016/j.electacta.2022.139838

Document Version
Publisher's PDF, also known as Version of record

Citation for published version (Harvard):
Oladeji, AV, Courtney, JM & Rees, NV 2022, 'Copper deposition on metallic and non-metallic single particles via impact electrochemistry', *Electrochimica Acta*, vol. 405, 139838. https://doi.org/10.1016/j.electacta.2022.139838

Electrochimica Acta 405 (2022) 139838

Contents lists available at ScienceDirect

Electrochimica Acta

journal homepage: www.elsevier.com/locate/electacta

Copper deposition on metallic and non-metallic single particles via impact electrochemistry☆

Abiola V. Oladeji, James M. Courtney, Neil V. Rees*

School of Chemical Engineering, University of Birmingham, Edgbaston, Birmingham B15 2TT. United Kingdom

ARTICLE INFO

Article history:
Received 20 August 2021
Revised 25 November 2021
Accepted 2 January 2022
Available online 3 January 2022

Keywords:
Impact electrochemistry
Underpotential deposition
Fly-ash cenospheres
Copper deposition

ABSTRACT

This study demonstrates the possibility of depositing metals onto low-metal content particles via impact electrochemistry, a technique used to measure transient current signals (electrochemical impacts) produced from the collision between particles moving under Brownian motion and a potentiostated interface (Rees, 2014; Markham et al., 2020; Zhang and Zhou, 2020). The deposition of copper onto the surface of fly-ash cenospheres via electrochemical impacts is reported, along with its deposition onto silver and gold nanoparticles. A comparison with linear sweep voltammetry confirmed that impact signals correlated with deposition potentials (bulk and underpotential deposition). Reductive impact events were observed at potentials negative of −0.3 V (for Ag) and −0.1 V (for Au) (vs. MSE), with evidence for a change in coverage of deposition from ca. 103% at −0.1 V to 261% at −0.8 V vs. MSE for Au. Cenospheres were shown to be sufficiently electrochemically active to facilitate copper deposition, either on modified electrodes or showing transient impact spikes indicating copper deposition, which was confirmed via SEM/EDX and ICP-MS analysis.

1. Introduction

The recovery of critical and commercially significant metals from waste streams is an essential aspect of their continuing and future sustainable use. Current methods of extraction are often not economically viable for low concentrations of critical metals, resulting in wide variations in recycling percentages for different metals [4,5]. Additionally, conventional methods of recovery such as chemical precipitation, adsorption/biosorption and ion exchange [6,7] are limited by large reagent consumption, secondary pollution generation and high operating costs [8,9]. Therefore, electrochemical methods such as electrodeposition, electrosorption, and electrodialysis [10], would appear to be well-suited for the recovery and recycling of many metals, provided a suitable solvent and reduction potential is used. The primary advantage of these techniques are the high efficiency, operational feasibility and cost effectiveness [11–13]. Electrodeposition is considered the most practical metal recovery technique with broad industrial applications [9,14–19] as it has the possibility of enabling selective metal recovery from aqueous solutions under mild conditions, however the removal of the deposited metal from the cathode is normally required for onward processing, and can create complications. Particle impact electrochemistry potentially has several advantages, for example the high rate of mass transport to nanoparticles, the potential for a large (tunable) number of nanoelectrodes being less susceptible to becoming fouled by contaminants that a single large electrode, and in particular the ability to choose a suitable core particle on which to deposit the metal being recovered in such a way as to either facilitate onward processing or directly produce desirable core-shell architectures. There are two potential uses of the particle-impact recovery method: first, where the particles are separated after deposition for further processing, and secondly where the deposition can be controlled sufficiently such the resulting core-shell particles can be separated and then used directly as catalysts, etc. Clearly the former case does not afford significant advantages over the existing method of deposition onto a cathode since the recovered metal still needs separation from the cathode material; but the second scenario would hold significant benefits ion the overall recovery-recycling process, and it is this long-term aim of the use of impacts for recovery/recycling.

☆ An article for submission to: Electrochimica Acta

* Corresponding author.
E-mail address: n.rees@bham.ac.uk (N.V. Rees).

https://doi.org/10.1016/j.electacta.2022.139838

During impact voltammetry, particles are introduced to a solution where they move under Brownian motion until collision with a substrate electrode held at a potential [20–23]. Upon collision, the particles can either undergo oxidation or reduction ('direct impacts') or provide a surface for solution species to be oxidised or reduced ('indirect impacts'), provided a suitable potential is applied to the substrate electrode. Both direct [24–34] and indirect [35–42] impact techniques result in transient current signals that can be analysed to examine the system under study elucidating information such as particle size, concentrations, and kinetics [20,43–48]. The electrodeposition of metals onto particles via impact electrochemistry has been reported in the literature, with examples including underpotential deposition (upd) and bulk deposition [49 – 51], although to date this has focussed on metallic core particles (Ag, Au). The use of non-precious metal cores would promote long-term sustainability and potential economic viability of any application in recovery/recycling and so there is interest in the possibility of using lower value (especially 'waste') materials as core particles. When considering the electrodeposition of metal(s) onto core particles via the impact method it is preferable, wherever possible, to select the substrate electrode material to be one with a significantly higher overpotential for the metal deposition, compared to that of the core particle material. This ensures that deposition will preferentially occur on the impacting particle and not the underlying substrate electrode. Where the difference in deposition overpotential is small, then deposition onto the substrate electrode may occur and compete with deposition onto the particle. Clearly, the former case is desired and a requirement of any use of this method for scaled-up application. Hence the use of the impact technique will be necessarily limited to combinations of metal solution species for recovery and particle-substrate materials with appropriately different deposition potentials. Furthermore, since the charge transferred (and hence amount of metal deposited) onto a particle during a single impact is small (dependant on the metal, particle size, deposition kinetics, applied potential etc.), it is likely that significant optimisation would be required to achieve near-total recovery of metal from solution within a realistic timeframe (for example via manipulating the rate of collisions, particle concentration, use of convection, etc.).

Cenospheres are a component of coal fly ash (CFA) which is generated in large quantities during the combustion of pulverised coal [52]. As such, they are considered waste and could be a useful functional recovered waste material, and in addition their low density makes their separation from the reaction solution relatively simple (via filtration or centrifugation, etc.). Cenospheres have been reported as a substrate for metal deposition, with Shukla et al. investigating the electroless deposition of Cu onto cenospheres via a layer of Pd clusters [53], with the primary objective of increasing conductivity and producing light weight metal matrix composites. Suggested applications for copper coated cenosphere particles involve the fabrication of conducting polymers and lead base composite material [53,54]. The modification of cenospheres using other techniques such as precipitation and fluidised-bed chemical vapour deposition [55,56] have also been documented. However, their suitability as substrate for direct electrochemical deposition is unclear due to their varying composition that is typically dominated by aluminosilicates and metal oxides [57–59]. A detailed characterisation is therefore required in each circumstance to determine factors such as chemical composition, morphology, and size distribution.

To investigate the suitability of impact electrochemistry for recycling applications, it was decided to study the deposition onto metallic nanoparticles, such as gold and silver nanoparticles (AuNPs, AgNPs), before extending the investigation to include the non-metallic recovered waste material, fly-ash cenospheres (FACs). Copper was selected as an electrochemically recyclable [60] commodity metal that undergoes a 2-electron reduction. Additionally, copper has relatively well-established voltammetry exhibiting a well-known upd region on gold [61–70], hence enabling demonstration of the technique.

2. Experimental

All chemicals used were obtained commercially and used without further purification, namely: copper sulphate (98%, Sigma Aldrich), potassium sulphate (99.0%, Sigma Aldrich) sulphuric acid (95.0–98.0%, Alfa Aesar), hexaammineruthenium (III) chloride (99.0%, Sigma Aldrich), potassium chloride (99.0–100.0%, Alfa Aesar), nitric acid (70.0%, Fisher Scientific), 60 nm silver nanoparticles (AgNPs, Nanocomposix Inc, USA), 50 nm and 60 nm gold nanoparticles (AuNPs, Nanocomposix Inc) and fly-ash cenospheres (FACs, RockTron International Ltd). All solutions were made using ultrapure water of resistivity $\geq$ 18.2 MΩ cm (MilliQ, Millipore).

Electrochemical experiments were performed using a three-electrode cell in a faraday cage. A glassy carbon (GC, diameter = 3 mm, BASi Inc) macroelectrode, and carbon fibre (CF) microelectrodes of different sizes (diameter = 9, 11, or 33 μm) were used as working electrodes. Carbon substrate electrodes were used for impact studies since they have a high overpotential for hydrogen evolution (unlike Pt), are not easily oxidised (cf. Ag), and Cu does not readily deposit onto it (cf. Au). The 9 μm electrodes were made in-house using pitch-derived carbon fibres (Goodfellow Cambridge Ltd), whilst the 11 μm and 33 μm electrodes were purchased (BASi Inc and ALS Inc respectively). Working electrodes were prepared by polishing the surface with alumina suspensions of 1 µm, 0.3 µm and 0.05 µm sequentially, on a micro-cloth pad (all from Buehler Inc, USA). A mercury sulphate electrode (MSE, IJ Cambria Ltd) was used as a reference electrode and a graphite rod (3 mm diameter, Goodfellow Cambridge Ltd) as the counter electrode. For nanoparticle experiments, the MSE reference electrode was placed in a separate fritted compartment to avoid possible cross-contamination. Unless otherwise stated a solution of 19 mM potassium sulphate, 1 mM sulphuric acid and, when required, an additional 0.5 mM copper sulphate was used. Solutions were thoroughly degassed using nitrogen gas (oxygen-free, BOC Gases plc) and a nitrogen atmosphere maintained throughout the experiments. Standard electrochemical measurements were conducted using an Autolab 128 N (Metrohm-Autolab BV, Netherlands) potentiostat controlled via a PC running NOVA 2.1 software conducting both linear sweep voltammetry and chronoamperometry scans. Impact chronoamperometric scans were measured using a bespoke low-noise potentiostat analogous to that described in [71], fitted with a high-speed variable-gain low-noise current amplifier (DHPCA-100, femto.de) with a bandwidth of 220 kHz and rise time of 1.6 μs at the operating gain of 10^8, and a data acquisition card (NI-6003, National Instruments, bandwidth 300 kHz) which combined enabled a sampling rate of 100 kS s^{-1}. All data was processed using a combination of Microsoft Excel and Origin Pro 2021. Unless stated otherwise, impact electrochemical data has been analysed following electronic filtration (digital) at 250 Hz in order to improve the signal-to-noise ratio and facilitate analysis (see Supplementary Information Section A). Where closer analysis was required, the 'raw' data was then reviewed when considering duration or peak current (see Supplementary Information for effects of filtration and Ref. [72]). Even then, any analysis of the data is semi-quantitative at best and requires appropriate caution since data acquisition is limited by the sampling rate (here 100 kS s^{-1}). Hence we have limited any use to comparing between for example, deposition on AuNPs and AgNPs in a relative sense rather than relying on interpreting absolute values. The design of the potentiostat is such that charge is conserved by the filter, as demonstrated elsewhere [72,73].

The cenospheres were characterised using a handheld X-ray fluorescence spectrometer (hXRF) [74], scanning electron microscopy (SEM) with energy dispersive X-ray (EDX) analysis and inductively coupled plasma mass spectrometry (ICP-MS). For the SEM/EDX characterisation, 5 mg of cenospheres were added to the surface of a carbon tape (Agar Scientific) then examined using the Hitachi TM3030 electron microscope. To analyse cenospheres where deposition had occurred, the solution post-chronoamperometric experiment was taken and drop-cast onto glassy carbon stubs, dried, rinsed thoroughly with deionised water and dried again to be studied in the same way with the SEM/EDX. Additional experiments were conducted where modified cenospheres processed as described below for ICP-MS were taken dry and analysed directly with the SEM/EDX.

ICP-MS analysis was conducted on both unmodified cenosphere particles and cenosphere particles that had been modified via a 12 hr chronoamperometric scan in 0.5 mM copper sulphate, 19 mM potassium sulphate and 1 mM sulphuric acid. The modified cenosphere sample was repeatedly centrifuged (SIGMA 3k30 centrifuge) at 5000 rpm for 10 min, rinsed with ultrapure water and sonicated (U-series, Ultrawave), then repeating the washing cycle, before allowing to dry. Both samples were prepared for ICP-MS by dissolving in 2% nitric acid at a concentration of 1 ppm (cenosphere content) for 48 hr before filtration with 0.45 μm syringe filters (Starlab Group Ltd). The solution was then analysed using an ICP-MS (Nexion 300X ICP-MS, Perkin Elmer) with a limit of detection of 0.174 ppb. A calibration curve was generated with 1 ppm copper standard for ICP-MS, (TraceCERT Sigma Aldrich) in ultrapure water at concentrations of 0.001 ppm to 0.01 ppm. The sample was then analysed and the concentration of copper read from the calibration curve.

3. Results and discussion

3.1. Impact deposition of Cu onto metallic nanoparticles

Macro and microelectrode studies were conducted to determine the onset potential of copper deposition onto GC and CF electrodes, as well as AuNP-modified GC and AgNP-modified GC electrodes before studying deposition onto FACs. Cyclic voltammograms (CVs) were taken of each electrode in a solution containing 0.5 mM copper sulphate, 19 mM potassium sulphate and 1 mM sulphuric acid at a voltage scan rate of 100 mV s^{-1}. For bare GC, CF, and AuNP-modified GC electrodes a start potential of 0.0 V vs. MSE was applied. Whereas, for the AgNP-modified GC the voltammetry scan started at −0.1 V vs. MSE to prevent the stripping of the AgNPs from the electrode surface. The onset potential can be defined as an adequately negative potential able to initiate a current response [75–77], in this case a current density of −0.025 A m^{-2} is used to determine onset potential.

Fig. 1. illustrates the reductive scans for GC, AuNP/GC, AgNP/GC, and CF working electrodes. Both the AuNP/GC and AgNP/GC surfaces were prepared via a drop-cast method also used by Tschulik et al. [78] where 5 µL of a suspension containing 50 nm AuNPs (or 50 nm AgNPs) was added to a polished GC surface. It can be observed that copper deposition on the gold-modified GC surface commences at a potential of −0.1 V vs. MSE whereas the onset onto other materials occurs at more negative potentials. This is due to underpotential deposition (upd) indicated by the characteristic initial peak at ca. −0.30 V vs. MSE, in agreement with the upd peak potential 0.05 V vs. Cu/Cu^{2+}onset reported in literature [62,64], where $E_{Cu/Cu^{2+}} = E_{SHE} + 0.28$ V [62] and $E_{SHE} = E_{MSE} - 0.64$ V giving a potential of −0.31 V vs. MSE. The deposition of copper onto a gold surface is well-documented and is categorised into four stages [64,77,79,80], namely the adsorption of copper and sulphate ions onto the gold surface, leading to a honeycomb ad-

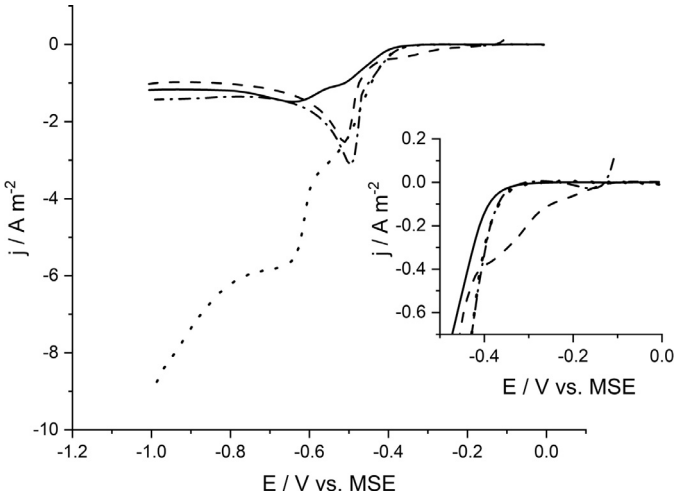

Fig. 1. depicts the reductive CV segments of copper deposition on the surface of 3 mm bare GC (—), 50 nm AgNP modified GC (-·-·-), 50 nm AuNP modified GC (— –) and 33 µm bare CF (·····). This was conducted in the standard copper plating solution of 0.5 mM $CuSO_4$, 1 mM H_2SO_4 and 19 mM K_2SO_4 using a scan rate of 100 mV s^{-1} in all cases.

layer, then a full copper upd monolayer, and finally bulk deposition. Fig. 1 is broadly in agreement with this, with the upd peak at ca. −0.3 V (vs. MSE) and bulk deposition occurring at potentials more negative than ca. −0.4 V (vs. MSE). From the upd peak an estimated AuNP surface coverage of ca. 0.5 layer equivalents was calculated based on the maximum possible available NP surface area (see Supplementary Information Section B Eqs. (1)–(6) and Table T1 for details).

To investigate whether electrochemical impact events for copper deposition occurs, chronoamperometry was conducted with and without the addition of nanoparticles to the copper sulphate solution described above for the same potentials. Fig. 2A depicts a 20 s segment of the chronoamperometric scans where peaks can be observed. This scan was performed at −0.8 V (vs. MSE) before and after the addition of silver nanoparticles. Upon the addition of silver nanoparticles, reductive transient peaks can be observed (see Fig. 2B) suggesting the occurrence of copper deposition during impact events at this potential. It is also noted that the background current varies quite widely, especially at more negative potentials, which we postulate to be due to small numbers of adsorbed nanoparticles and the deposition behaviour of copper (please see Supplementary Information Section C for more detail).

Further investigations were then conducted to determine the potential window at which the impact events could be observed, by recording chronoamperograms at a range of potentials under potentiostatic control. Fig. 2C shows the frequency of reductive peaks detected at the different potentials ranging from −0.8 V to −0.1 V (vs. MSE), with the average frequencies at each potential where impacts were observed being in the range 2.3 to 3.7 GHz m^{-2}. Further details of the analysis are provided in the Supplementary Information (Section D). At potentials more negative than −0.3 V vs. MSE, reductive peaks can be observed. This agrees with the data shown in Fig. 1 (and in literature [61,81]) indicating that the onset of bulk copper deposition on the surface of silver is approximately −0.33 V (vs. MSE). The copper coverage of individual impacts was calculated using the charge determined from the integrated area of each peak (see Supplementary Information Section E):

$$S = 4\pi R^2 \quad (1)$$

$$Q = \int Idt = ezN \quad (2)$$

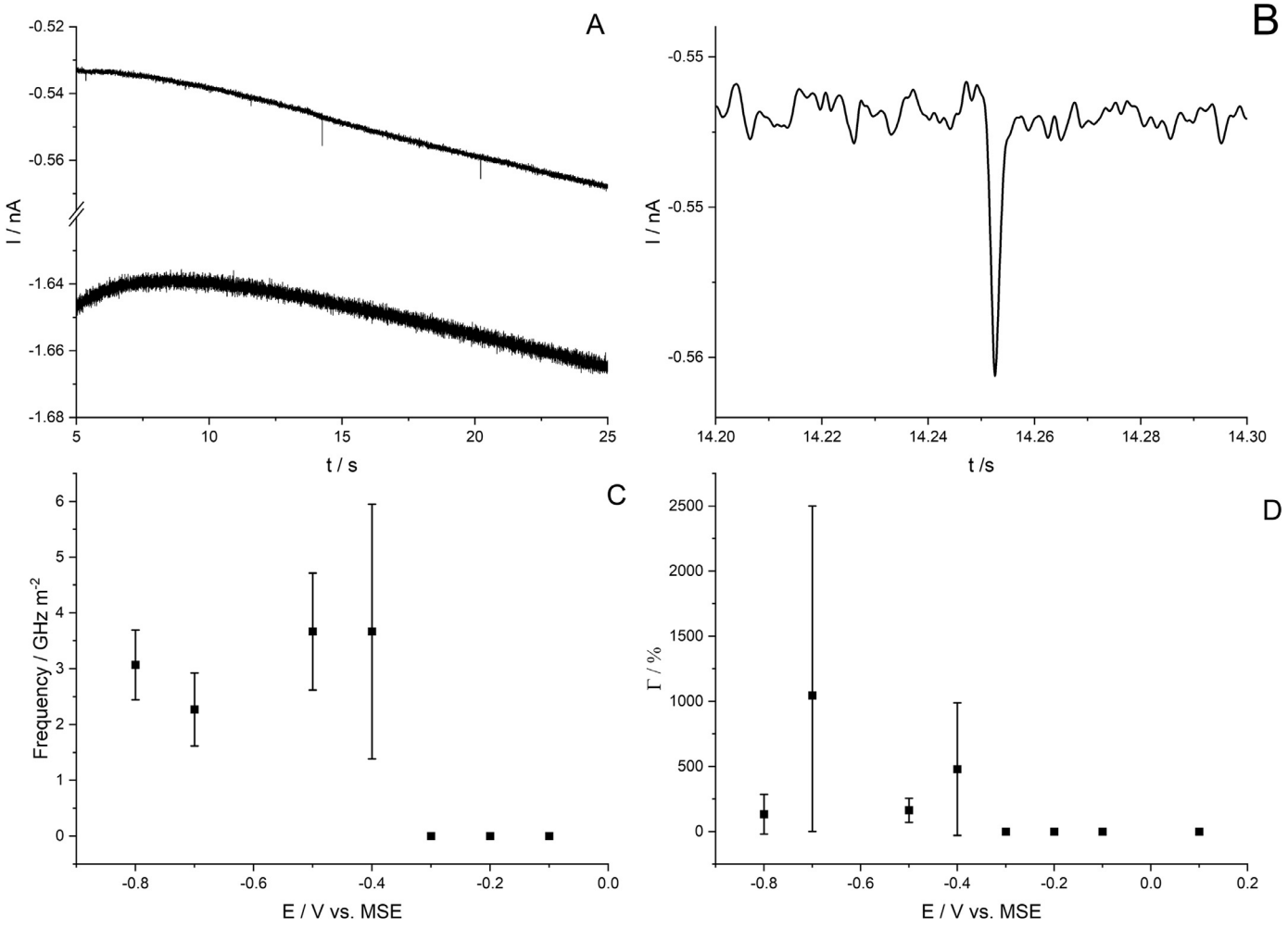

Fig. 2. A shows an illustrative depiction of a typical 20 s segment of chronoamperometric scans at −0.8 V vs. MSE before (i) and after (ii) the addition of 60 nm silver nanoparticles. Fig. 2B presents a magnified reductive peak from scan A (ii) at 14.25 s. All experiments were conducted in a 5 mL solution of 0.5 mM $CuSO_4$, 1 mM H_2SO_4 and 19 mM K_2SO_4 using a CF working electrode, a mercury sulphate reference electrode with a glass frit and a graphite rod counter electrode. Fig. 2C shows the frequency of impacts, normalised for electrode area, detected during 30 s chronoamperometric scans using a 20 pM suspension of 60 nm AgNPs at different potentials. Fig. 2D displays the calculated average coverage of impacting AgNP at varying potentials where copper deposition occurred on nanoparticle collisions occurring at a potential negative of −0.3 V vs. MSE.

$$N_{mono} = 0.7405\ \frac{S}{\pi r^2} \tag{3}$$

$$\theta = \frac{Q}{5.924}\left(\frac{r}{R}\right)^2 \tag{4}$$

where S is the nanoparticle surface area, R the NP radius, Q the associated reductive charge, t the spike duration, e the electronic charge, $z = 2$ the number of exchanged electrons per reduced copper atom [30], θ the coverage, $r = 1.96$ Å the copper atomic radius [82], N the number of reduced copper atoms and N_{mono} the number of copper atoms in a monolayer based on a 74.05% fcc surface coverage [83]. The average coverage was calculated for impacts at different potentials (see Fig. 2D). The data suggests that coverage greater than a monolayer equivalent occurs once the applied potential is negative of the 'switch on' potential, for example at −0.4 V vs. MSE, an average coverage of 479% was observed.

Analogous impact experiments were then conducted using a 20 pM suspension of AuNPs to study whether impacts were observed in the upd and bulk deposition regions in Fig. 1. Similar to the AgNP system, upon the addition of AuNPs, reductive transient peaks could be observed for a range of potentials vs. MSE. Fig. 3A displays the chronoamperometric scans before and after the addition of gold nanoparticles conducted at −0.3 V (upd region) and at −0.8 V (bulk deposition region). It can be observed that before the addition of AuNPs the scan is void of transient peaks, however upon the addition of gold nanoparticles reductive peaks are observed at both −0.3 V and −0.8 V (vs. MSE.), in the upd and bulk deposition regions.

The impact 'spikes' were integrated to obtain the charge passed during each impact, allowing calculation of the percentage coverage of the deposit, assuming a spherical NP, using Eqs. (1)–(4) [49–51]. Fig. 3B illustrates the calculated percentage coverage of impacting AuNP at varying potentials ranging from −0.8 V to 0.1 V (vs. MSE). Peaks begin to occur at potentials more negative than −0.1 V vs. MSE. This is in good agreement with the onset potential determined (see Fig. 1) and the upd region reported in [63]. The data shows that at potentials where upd is expected, the impacts observed correspond to an average coverage of ca.103% ± 8%, the theoretical monolayer coverage. On the other hand, at more negative potentials where bulk deposition would occur, the maximum percentage coverage is higher with an average coverage of 215% ± 37%, significantly exceeding the equivalent of monolayer coverage.

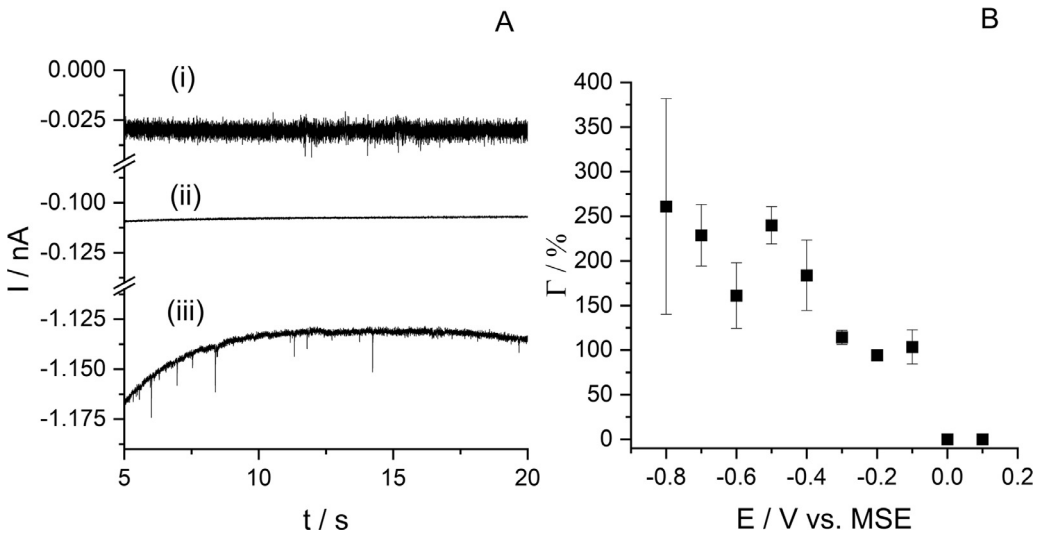

Fig. 0.3. A depicts a 15 s segment of three 30 s chronoamperometric scans (i) a chronoamperometric scan at −0.3 V using a 9 µm CF after the addition of AuNPs (ii) a scan conducted at a potential of −0.55 V using a 11 µm CF electrode before the addition of AuNPs (iii) a scan at −0.8 V using 11 µm CF after the addition of 60 nm AuNPs . Fig. 3B shows the calculated average percentage coverage (Γ) of individual 50 nm AuNP impacts at different potentials ranging from 0.1 V to −0.8 V vs. MSE. A series of 30 s chronoamperometric scans were conducted in a 5 mL solution of 0.5 mM $CuSO_4$, 1 mM H_2SO_4 and 19 mM K_2SO_4 using a CF working electrode, a mercury sulphate reference electrode with a glass frit and a graphite rod counter electrode.

A comparison of the AgNP and AuNP coverage (Figs. 2D and 3B) indicates a significantly higher copper coverage for the AgNP impacts. Given the similarity between bulk deposition onset, particles sizes (50–60 nm), and sticking coefficients for the AgNPs and AuNPs (0.15 for AgNPs [84], and 0.19 for AuNPs [85], reported for particles of mean radii ca 10–13 nm), it might be expected that the coverages should also be similar provided that the bulk deposition kinetics of Cu were not markedly different on Ag and Au. We postulate that the observed difference in deposition amounts is due to the degree of aggregation in the NPs, with AgNPs in particular, known to have rapid aggregation kinetics [27]. Since the coverage calculations are based on a single particle of mean diameter, they are highly sensitive to aggregation. Closer examination of the data indicates that the apparent coverages on Ag are skewed by several significantly larger impact spikes, which are consistent with the impacts of larger aggregates of NPs. Removal of these larger impacts yields coverages in the range 60–170% of a monolayer, which is comparable with the AuNP result.

3.2. Impact deposition of Cu onto fly-ash cenospheres (FACs)

After demonstrating the deposition of copper onto metallic nanoparticles, the reduction of copper onto cenosphere particles was investigated. Cenospheres were chosen as a core material for deposition as they are considered a waste product of the coal combustion process, additionally these are predominantly non-metallic particles. As previously stated, the composition of cenospheres varies and is influenced by the combustion conditions and coal composition [52,55]. As such, the cenosphere were characterised using SEM/ EDX, which enabled an approximate size distribution and composition to be obtained. Fig. 4B shows the particle size distribution produced from SEM images of the cenosphere sample and highlights a population centred around 1 µm in size, though a very large range of sizes occur, subsequent images and size analysis is shown in Supplementary Information Section F.

Impact electrochemistry primarily focuses on particles on the nanoscale. Within literature it has been observed that the impact electrochemistry technique is able to facilitate the detection of a wide variation of particles sizes with 6 nm reported as the lower limit of detection [86]. With regards to the upper limit, it has been suggested the application of direct impact is possible for sizing agglomerated particles beyond the upper nanoparticle limits (100 nm) as seen in [27,31,87]. The variation in cenosphere size and complex composition may affect the impact deposition process, as a result of the differing particle hydrodynamics under Brownian motion and settling properties [88]. Additionally, observations have been made suggesting an increase in the peak current with increasing particles size [89]. According to Zhou et al. [84,85], sticking potential is not significantly affected by size however does vary with the impacting material and substrate electrode [90,91].

Table 1
Average compositions by mass of FACs determined by SEM/EDX ($N = 7$).

Element	Average composition /%
Silicon	52.3
Aluminium	29.4
Iron	9.0
Calcium	6.7
Magnesium	2.3
Copper	0.2

The SEM/EDX analysis in Table 1 is in agreement with both the XRF data obtained and literature reports (see Supplementary Information Section G Table T4) that cenospheres are mainly comprised of metal oxides, with varying compositions reflecting those of their starting materials [57,92,93]. To determine the suitability of the cenospheres for electrochemical impact experiments, the deposition of copper onto the cenosphere particles were investigated by drop-casting to produce a cenosphere-modified GC macro electrode ($d = 3$ mm) with ca. 1900% coverage, based on calculation assuming even distribution [78]. Fig. 5 illustrates the reductive linear sweep voltammograms recorded for the bare GC and the FAC-modified GC electrode in a solution of 0.5 mM copper sulphate, 19 mM potassium sulphate and 1 mM sulphuric acid at a voltage scan rate of 100 mV s^{-1}. According to both Danilov et al. and Bimaghra and Crousier [94,95], the 2-electron deposition of copper onto carbonaceous materials occurs via the Volmer-Weber mechanism resulting in three-dimensional nucleation. Briefly, upon the establishment of the electric double layer, both copper metal adatoms and univalent copper ions accumulate near the electrode

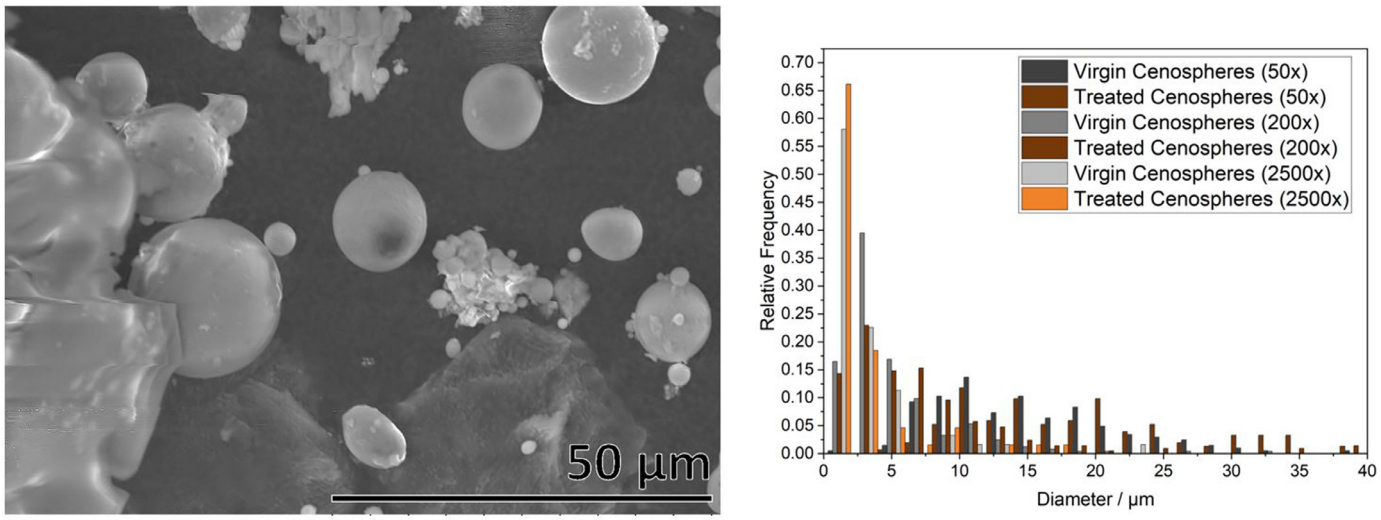

Fig. 4. A SEM image of impacted cenosphere particles with higher copper content. Fig. 4B Size distribution of FACs from SEM images using a magnification of 50x, 200x and 2500x, analysed using GIMP software ($N = 976$).

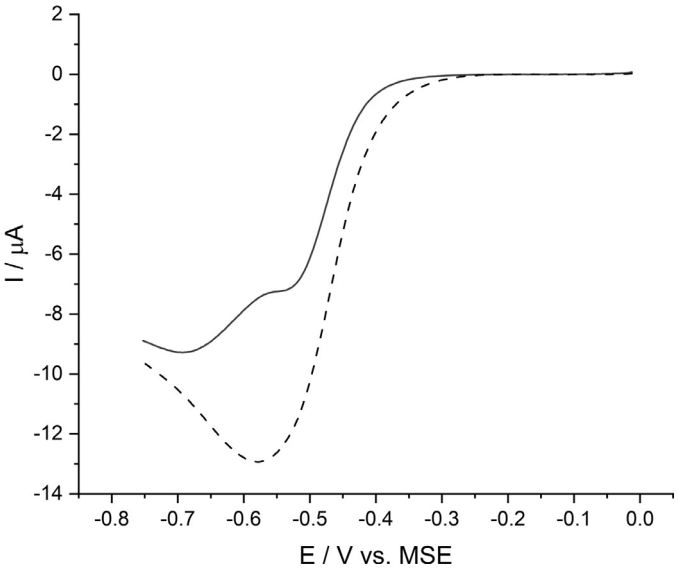

Fig. 5. illustrates the reductive scans of copper deposition on the surface of 3 mm Bare GC (—) and a cenosphere modified GC surface (––). A 100 mV s^{-1} scan rate was used between the potential window 0.0 V to −0.75 V (vs. MSE) in a solution of 0.5 mM $CuSO_4$, 1 mM H_2SO_4 and 19 mM K_2SO_4.

surface via the reactions:

$$Cu^{2+} + e \rightarrow Cu^{+}$$

$$Cu^{+} + e \rightarrow Cu_{ad}$$

where a quasi-equilibrium occurs between the Cu^{+} ions and free unbound Cu adatoms. As copper nuclei form at the surface of the electrode, the corresponding reductive current is influenced by cathodic overpotential, active surface area of the deposit and the mass transport of ions to the electrode/ solution and nuclei/solution interface. The cyclic voltammetry (see Fig. 5) for the bare GC depicts two peaks with currents of −7.2 µA and −2.1 µA where the first peak is ascribed to copper deposition on the bare GC (peak 1) followed by deposition on the copper-modified GC surface (peak 2).

Upon modification of the bare GC with cenosphere particles, the cenosphere-modified electrode has increased reductive current without any discernible increase in capacitance (see Supplementary Information Section G for detailed discussion on the effect on capacitance of cenosphere modification). This indicates the cenospheres have sufficient electrical conductivity such that the increased surface area of the electrode leads to an increased current response. In addition, Fig. 5 identifies the onset potential of copper deposition onto the surface of the cenosphere particles. From this it was determined peaks may be observed upon impact with the substrate electrode at a potential negative of −0.3 V vs. MSE.

Next, 0.05 g of FACs were added to 5 mL of a solution of 0.5 mM copper sulphate, 19 mM potassium sulphate, and 1 mM sulphuric acid resulting in a (number) concentration of 0.01 pM (see Supplementary Information Section G equations (8)-(9)) and agitated using the degassing nitrogen stream. A carbon fibre working electrode (33 μm) was used to investigate whether FAC impacts relating to Cu deposition could be observed. Fig. 6A displays typical chronoamperometric scans at −0.75 V vs. MSE in the copper solution before and after the addition of the cenosphere particles showing the emergence of reductive events on the addition of cenospheres to the system (see Fig. 6B). Note that positive-direction spikes that would be associated with the partial blocking of the background reductive current at the CF electrode are not observed [96]. Furthermore, chronoamperometric scans were conducted in a solution containing only 19 mM potassium sulphate and 1 mM sulphuric acid before and after the introduction of cenosphere particles (see Supplementary Information Section G, Fig. S12), and no impact spikes were observed. The blocking effect of the cenosphere particles were further investigated by conducting chronoamperometric scans in a solution of 0.5 mM $Ru(NH_3)_6Cl_3$, 1 mM H_2SO_4 and 19 mM K_2SO_4 with a 33 µm CF at −0.6 V (vs. SCE) before and after the addition of cenosphere particles. During the investigation it was possible to obtain a blank chronoamperometric scan without transient peaks before the addition of particles. Upon the addition of cenosphere particles a reductive peak could be observed suggesting an increase in current rather than a blocking effect. Again, positive-direction spikes corresponding with the partial blocking of current by the cenospheres particles are not observed (see Supplementary Information Section G, Fig. S13). The conclusion is therefore made that the reductive peaks observed in Fig. 6B are due to the deposition of copper on the impacting cenosphere particles.

To obtain direct evidence of Cu deposition onto the FACs, a 12 hr chronoamperometric scan was conducted using a 3 mm GC

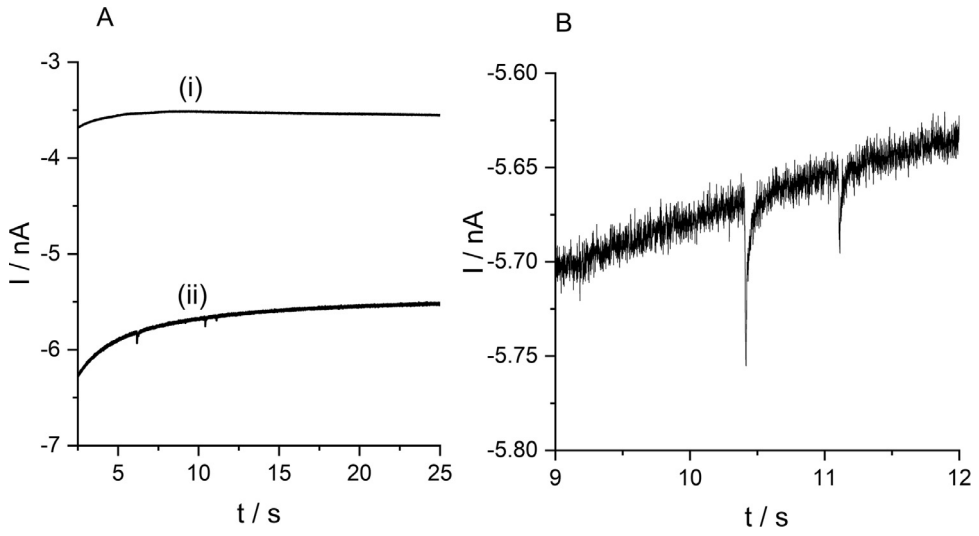

Fig. 6. A illustrates two chronoamperometric scans conducted in a 5 mL solution of 0.5 mM $CuSO_4$, 1 mM H_2SO_4 and 19 mM K_2SO_4 before (i) and after (ii) the addition of cenosphere particles. Both were performed at a potential of −0.75 V vs. MSE for 30 s. (B) highlights reductive peaks observed upon the addition of the cenosphere particles.

Table 2
displays the copper content determined by SEM/ EDX analysis of the background (GC stub), the unmodified cenosphere particles and impacted cenosphere particles. Copper content is presented as a ratio of copper and silicon count.

Sample	Percentage copper content ratio /%
Background (GC stub surface)	0
Pristine cenosphere particles	0.07 ± 0.08
Impacted cenosphere particles	7.43 ± 2.47

electrode at −0.75 V vs. MSE in a solution containing 0.5 mM copper sulphate, 19 mM potassium sulphate, 1 mM sulphuric acid and 0.05 g cenosphere particles. This solution was then agitated briefly using the degassing nitrogen gas stream before commencing the chronoamperometric scan. Upon completion, 5 µL of the reacted suspension solution was extracted from the reaction cell, drop-cast onto a polished GC stub and then analysed using SEM/EDX to determine the copper content of the cenospheres (additional experiments used dried cenospheres obtained through rinsing cycles and centrifugation as described in ICP-MS sample preparation). Table 2 shows the average copper content of the impacted cenospheres determined using SEM/ EDX analysis confirming that the average Cu content of impacted FACs is significantly higher than for non-impacted (pristine) FACs, with an average Cu content of 7.43 ± 2.47% compared to 0.07 ± 0.08% (by count, $N = 7$). Note that these values are quoted relative to the measured silicon (Si) content of the same FAC particle, to account for the variation in particle size and composition. Detecting cenospheres with copper deposition in the solution sample demonstrates that after impacting the GC electrode the some particles are able to detach from the surface. An SEM analysis of the GC stub was also conducted and indicated a build-up of copper deposition with cenosphere inclusions (see Supplementary Information Section H). The degree of deposition of Cu onto the GC substrate, will clearly be dependant on the potential at which the impact experiment was conducted, and here was expected due to the choice of deposition potential. Detailed quantitative analysis of the degree of deposition onto the GC stub (via XPS) was not conducted here, since this was outside the scope of this study. However, such detailed analysis of the substrate electrode would be necessary when considering quantitative application of the impact technique for scaled-up application.

The SEM analysis also identified some cenospheres present with a similar (near zero) level of copper content to the control, implying not all cenospheres collided with the GC electrode or else an impact occurred with little to no copper deposition. This variation is expected as the impact deposition process is uncontrolled, and the cenosphere composition (and hence conductivity) is not uniform (additional imagery and copper content analysis is shown in Supporting Information Section H).

In addition to the SEM/EDX analysis, ICP-MS analysis of both the impacted and the unmodified cenosphere particles was conducted. The analysis showed that the unmodified cenosphere had a copper content in the sample of 1.0 ppb and the modified cenosphere sample had double the copper content at 2.0 ppb. These values are well above the detection limit (0.174 ppb) of the ICP-MS and as such provides further evidence of impacting cenosphere increasing in concentration of copper.

4. Conclusion

The macro- and microelectrode studies demonstrated that the onset for copper deposition varied depending on the substrate material agreeing with previous literature [65,97]. A drop-casting technique was employed to show upd occurred for copper on gold further agreeing with literature [64]. Using impact voltammetry, copper deposition was observed during silver nanoparticle impacts, where the switch on/ off potential aligned with the onset potential previously mentioned at −0.4 V vs. MSE. Studies with AuNPs indicated the impact switch on/ off for copper deposition on gold shifted positively thus reflecting the upd onset predicted (to −0.1 V vs. MSE). Evidence was found suggesting peaks occurring in the upd region resulted in particle coverage of approximately a monolayer (with an average of ca. 103% ± 8%) while peaks in the bulk region showed indication of a higher coverage (with an average of ca. 215% ± 37%).

Cenospheres were tested for use as a functional recovered waste material, the particles were characterised showing significant amounts of silicon and aluminium with lower amounts of iron, calcium, magnesium, and copper agreeing with previous literature. A size distribution analysis was conducted indicating a wide range of sizes from 100 s of nanometres to 100 s of microns with a population centred at 1 µm. The same drop-cast method was applied and showed that the cenosphere particles were electro-

chemically active. During impact voltammetry cenospheres exhibited transient spikes and evidence of copper deposition. This was supported by direct evidence found via SEM/ EDX and ICP-MS analysis showing copper had been deposited onto the cenosphere.

Declaration of Competing Interest

The authors declare that they have no known competing financial interests or personal relationships that could have appeared to influence the work reported in this paper.

Credit authorship contribution statement

Abiola V. Oladeji: Visualization, Formal analysis, Writing – original draft. **James M. Courtney:** Visualization, Formal analysis, Writing – review & editing. **Neil V. Rees:** Supervision, Writing – review & editing.

Acknowledgments

This work was funded by the Leverhulme Trust (RPG-2019–146), and additionally AVO thanks the EPSRC CDT for fuel cells and their fuels (EP/G037116/1) for a studentship. The authors thank Prof. N.A. Rowson and Dr. R. Sommerville for XRF spectroscopy, Dr C. Stark for assistance with ICP-MS, and Dr. C. Stoppiello (University of Nottingham) for discussions on XPS.

Supplementary materials

Supplementary material associated with this article can be found, in the online version, at doi:10.1016/j.electacta.2022.139838.

References

[1] N.V. Rees, Electrochemical insight from nanoparticle collisions with electrodes: a mini-review, Electrochem. Commun. 43 (2014) 83.
[2] J. Markham, N.P. Young, C. Batchelor-McAuley, R.G. Compton, Bipolar nanoimpact transients: controlling the redox potential of nanoparticles in solution, J. Phys. Chem. C 124 (2020) 14043.
[3] J.H. Zhang, Y.G. Zhou, Nano-impact electrochemistry: analysis of single bioentities, TrAC Trends Anal. Chem. 123 (2020) 115768.
[4] K. Nose, T.H. Okabe, S. Seetharaman, Platinum group metals production, in: Treatise On Process Metallurgy, 3, Elsevier, 2014, p. 1071. Vol.Ch. 2.10.
[5] C. Hagelüken, G. Gunn, Recycling of (critical) metals, in: Critical Metals Handbook, Wiley, 2014, p. 41. Ch. 3.
[6] A.S. Sheoran, V. Sheoran, Heavy metal removal mechanism of acid mine drainage in wetlands: a critical review, Miner. Eng. 19 (2006) 105.
[7] M.A. Barakat, New trends in removing heavy metals from industrial wastewater, Arab. J. Chem. 4 (2011) 361.
[8] H. Lu, Y. Wang, J. Wang, Recovery of Ni^{2+} and pure water from electroplating rinse wastewater by an integrated two-stage electrodeionization process, J. Clean. Prod. 92 (2015) 257.
[9] T.A. Kurniawan, G.Y.S. Chan, W.H. Lo, S. Babel, Physico–chemical treatment techniques for wastewater laden with heavy metals, Chem. Eng. J. 118 (2006) 83.
[10] W. Jin, Y. Zhang, Sustainable electrochemical extraction of metal resources from waste streams: from removal to recovery, ACS Sustain. Chem. Eng. 8 (2020) 4693.
[11] N. Meunier, P. Drogui, C. Montané, R. Hausler, G. Mercier, J.F. Blais, Comparison between electrocoagulation and chemical precipitation for metals removal from acidic soil leachate, J. Hazard. Mater. 137 (2006) 581.
[12] C. Zhang, Y. Jiang, Y. Li, Z. Hu, L. Zhou, M. Zhou, Three-dimensional electrochemical process for wastewater treatment: a general review, Chem. Eng. J. 228 (2013) 455.
[13] T.K. Tran, H.J. Leu, K.F. Chiu, C.Y. Lin, Electrochemical treatment of heavy metal-containing wastewater with the removal of COD and heavy metal ions, J. Chin. Chem. Soc. 64 (2017) 493.
[14] K. Scott, E.M. Paton, An analysis of metal recovery by electrodeposition from mixed metal ion solutions—part II. Electrodeposition of cadmium from process solutions, Electrochim. Acta 38 (1993) 2191.
[15] A.G. Tyson, Chemelec' cell for recovery and recycling of metal in the electroplating industry, in: Proceedings of the 4th Heavy Metal Environment International Conference, 2, 1983, p. 988.
[16] L.A. Diaz, T.E. Lister, J.A. Parkman, G.G. Clark, Comprehensive process for the recovery of value and critical materials from electronic waste, J. Clean. Prod. 125 (2016) 236.
[17] K. Tanong, L.H. Tran, G. Mercier, J.F. Blais, Recovery of Zn (II), Mn (II), Cd (II) and Ni (II) from the unsorted spent batteries using solvent extraction, electrodeposition and precipitation methods, J. Clean. Prod. 148 (2017) 233.
[18] L. Zhang, Q. Song, Y. Liu, Z. Xu, An integrated capture of copper scrap and electrodeposition process to enrich and prepare pure palladium for recycling of spent catalyst from automobile, Waste Manag. 108 (2020) 172.
[19] I. Masavetas, A. Moutsatsou, E. Nikolaou, S. Spanou, A. Zoikis-Karathansis, E.A. Pavlatou, N. Spyrellis, Production of copper powder from printed circuit boards by electrodeposition, Glob. Nest J. 11 (2009) 241.
[20] P.H. Robbs, N.V. Rees, Nanoparticle electrochemistry, Phys. Chem. Chem. Phys. 18 (2016) 24812.
[21] L.K. Allerston, N.V. Rees, Nanoparticle impacts in innovative electrochemistry, Curr. Opin. Electrochem. 10 (2018) 31.
[22] J.M. Kahk, N.V. Rees, J. Pillay, R. Tshikhudo, S. Vilakazi, R.G. Compton, Electron transfer kinetics at single nanoparticles, Nano Today 7 (2012) 174.
[23] A.V. Korshunov, M. Heyrovský, Voltammetry of metallic powder suspensions on mercury electrodes, Electroanalysis 18 (2006) 423.
[24] E.N. Saw, N. Blanc, K. Kanokkanchana, K. Tschulik, Time-resolved impact electrochemistry - a new method to determine diffusion coefficients of ions in solution, Electrochim. Acta 282 (2018) 317.
[25] M. Pumera, Impact electrochemistry: measuring individual nanoparticles, ACS Nano 8 (2014) 7555.
[26] Y.G. Zhou, N.V. Rees, R.G. Compton, The electrochemical detection and characterization of silver nanoparticles in aqueous solution, Angew. Chem. Int. Ed. Engl. 50 (2011) 4219.
[27] N.V. Rees, Y.G. Zhou, R.G. Compton, The aggregation of silver nanoparticles in aqueous solution investigated via anodic particle coulometry, ChemPhysChem 12 (2011) 1645.
[28] B. Haddou, N.V. Rees, R.G. Compton, Nanoparticle-electrode impacts: the oxidation of copper nanoparticles has slow kinetics, Phys. Chem. Chem. Phys. 14 (2012) 13612.
[29] Y.G. Zhou, B. Haddou, N.V. Rees, R.G. Compton, The charge transfer kinetics of the oxidation of silver and nickel nanoparticles via particle-electrode impact electrochemistry, Phys. Chem. Chem. Phys. 14 (2012) 14354.
[30] K. Tschulik, B. Haddou, D. Omanović, N.V. Rees, R.G. Compton, Coulometric sizing of nanoparticles: cathodic and anodic impact experiments open two independent routes to electrochemical sizing of Fe_3O_4 nanoparticles, Nano Res. 6 (2013) 836.
[31] M.Z.M. Nasir, M. Pumera, Impact electrochemistry on screen-printed electrodes for the detection of monodispersed silver nanoparticles of sizes 10–107nm, Phys. Chem. Chem. Phys. 18 (2016) 28183.
[32] W.Z. Teo, M. Pumera, Fate of silver nanoparticles in natural waters; integrative use of conventional and electrochemical analytical techniques, RSC Adv. 4 (2014) 5006.
[33] E.J.E. Stuart, Y.G. Zhou, N.V. Rees, R.G. Compton, Determining unknown concentrations of nanoparticles: the particle-impact electrochemistry of nickel and silver, RSC Adv. 2 (2012) 6879.
[34] C.S. Lim, M. Pumera, Impact electrochemistry: colloidal metal sulfide detection by cathodic particle coulometry, Phys. Chem. Chem. Phys. 17 (2015) 26997.
[35] S.J. Kwon, A.J. Bard, Analysis of diffusion-controlled stochastic events of iridium oxide single nanoparticle collisions by scanning electrochemical microscopy, J. Am. Chem. Soc. 134 (2012) 7102.
[36] X. Xiao, F.R. Fan, J. Zhou, A.J. Bard, Current transients in single nanoparticle collision events, J. Am. Chem. Soc. 130 (2008) 16669.
[37] Y.G. Zhou, N.V. Rees, R.G. Compton, The electrochemical detection of tagged nanoparticles via particle-electrode collisions: nanoelectroanalysis beyond immobilisation, Chem. Commun. 48 (2012) 2510.
[38] S.J. Kwon, F.-R.F. Fan, A.J. Bard, Observing iridium oxide (IrO(x)) single nanoparticle collisions at ultramicroelectrodes, J. Am. Chem. Soc. 132 (2010) 13165.
[39] S.J. Kwon, H. Zhou, F.-R.F. Fan, V. Vorobyev, B. Zhang, A.J. Bard, Stochastic electrochemistry with electrocatalytic nanoparticles at inert ultramicroelectrodes-theory and experiments, Phys. Chem. Chem. Phys. 13 (2011) 5394.
[40] Y.G. Zhou, N.V. Rees, R.G. Compton, Electrochemistry of nickel nanoparticles is controlled by surface oxide layers, Phys. Chem. Chem. Phys. 15 (2013) 761.
[41] E.J.E. Stuart, N.V. Rees, R.G. Compton, Particle-impact voltammetry: the reduction of hydrogen peroxide at silver nanoparticles impacting a carbon electrode, Chem. Phys. Lett. 531 (2012) 94.
[42] N.V. Rees, Y.G. Zhou, R.G. Compton, Making contact: charge transfer during particle-electrode collisions, RSC Adv. 2 (2012) 379.
[43] N.V. Rees, Electrochemical insight from nanoparticle collisions with electrodes: a mini-review, Electrochem. Commun. 43 (2014) 83.
[44] E.J.E. Stuart, Y.G. Zhou, N.V. Rees, R.G. Compton, Particle-impact nanoelectrochemistry: a Fickian model for nanoparticle transport, RSC Adv. 2 (2012) 12702.
[45] W. Cheng, X.F. Zhou, R.G. Compton, Electrochemical sizing of organic nanoparticles, Angew. Chem. Int. Ed. 52 (2013) 12980.
[46] W. Cheng, C. Batchelor-McAuley, R.G. Compton, Organic nanoparticles: mechanism of electron transfer to indigo nanoparticles, ChemElectroChem 1 (2014) 714.
[47] X. Xiao, A.J. Bard, Observing single nanoparticle collisions at an ultramicroelectrode by electrocatalytic amplification, J. Am. Chem. Soc. 129 (2007) 9610.
[48] M. Giovanni, A. Ambrosi, Z. Sofer, M. Pumera, Impact electrochemistry of individual molybdenum nanoparticles, Electrochem. Commun. 56 (2015) 16.
[49] G. Zampardi, R.G. Compton, Fast electrodeposition of zinc onto single zinc nanoparticles, J. Solid State Electrochem. 24 (2020) 2695.
[50] Y.G. Zhou, N.V. Rees, R.G. Compton, Nanoparticle-electrode collision processes:

the underpotential deposition of thallium on silver nanoparticles in aqueous solution, ChemPhysChem 12 (2011) 2085.
[51] Y.G. Zhou, N.V. Rees, R.G. Compton, Nanoparticle–electrode collision processes: the electroplating of bulk cadmium on impacting silver nanoparticles, Chem. Phys. Lett. 511 (2011) 183.
[52] S.V. Vassilev, C.G. Vassileva, Methods for characterization of composition of fly ashes from coal-fired power stations: a critical overview, Energy Fuels 19 (2005) 1084.
[53] S. Shukla, S. Seal, J. Akesson, R. Oder, R. Carter, Z. Rahman, Study of mechanism of electroless copper coating of fly-ash cenosphere particles, Appl. Surf. Sci. 181 (2001) 35.
[54] X. Yu, Z. Xu, Z. Shen, Metal copper films deposited on cenosphere particles by magnetron sputtering method, J. Phys. D Appl. Phys. 40 (2007) 2894.
[55] Y.T. Yu, Preparation of nanocrystalline TiO_2-coated coal fly ash and effect of iron oxides in coal fly ash on photocatalytic activity, Powder Technol. 146 (2004) 154.
[56] W. Żukowski, P. Migas, D. Bradło, P. Dulian, Synthesis and performance of TiO_2/fly ash cenospheres as a catalytic film in a novel type of periodic air-sparged photocatalytic reactor, Materials 13 (2020) 1691 (Basel).
[57] R.S. Blissett, N.A. Rowson, A review of the multi-component utilisation of coal fly ash, Fuel 97 (2012) 1.
[58] N. Moreno, X. Querol, J.M. Andrés, K. Stanton, M. Towler, H. Nugteren, M. Janssen-Jurkovicová, R. Jones, Physico-chemical characteristics of European pulverized coal combustion fly ashes, Fuel 84 (2005) 1351.
[59] B. Kim, M. Prezzi, Evaluation of the mechanical properties of class-F fly ash, J. Waste Manag. 28 (2008) 649.
[60] K. Scott, X. Chen, J.W. Atkinson, M. Todd, R.D. Armstrong, Electrochemical recycling of tin, lead and copper from stripping solution in the manufacture of circuit boards, Resour. Conserv. Recycl. 20 (1997) 43.
[61] M. Dietterle, T. Will, D.M. Kolb, The initial stages of copper deposition on Ag(111): an STM study, Surf. Sci. 342 (1995) 29.
[62] Z. Shi, S. Wu, J. Lipkowski, Coadsorption of metal atoms and anions: cu upd in the presence of SO_4^{2-}, Cl– and Br–, Electrochim. Acta 40 (1995) 9.
[63] I.H. Omar, H.J. Pauling, K. Jüttner, Underpotential deposition of copper on Au(III) single-crystal surfaces: a voltammetric and rotating ring disk electrode study, J. Electrochem. Soc. 140 (1993) 2187.
[64] M.A. Schneeweiss, D.M. Kolb, The initial stages of copper deposition on bare and chemically modified gold electrodes, Phys. Status Solidi A 173 (1999) 51.
[65] E. Herrero, L.J. Buller, H.D. Abruña, Underpotential deposition at single crystal surfaces of Au, Pt, Ag and other materials, Chem. Rev. 10 (2001) 1897.
[66] K. Jüttner, W.J. Lorenz, Underpotential metal deposition on single crystal surfaces, Z. Phys. Chem. 122 (1980) 163.
[67] S. Szabos, Underpotential deposition of metals on foreign metal substrates, Int. Rev. Phys. Chem. 10 (1991) 207.
[68] M. Cappadonia, U. Linke, K.M. Robinson, J. Schmidberger, U. Stimming, Anion effects on the cyclic voltammetry of copper underpotential deposition on Au(100), J. Electroanal. Chem 405 (1996) 227.
[69] E.B. Budevski, G.T. Staikov, W.J. Lorenz, Electrochemical phase formation and growth, An Introduction to the Initial Stages of Metal Deposition, John Wiley & Sons, 2008.
[70] D.M. Kolb, M. Przasnyski, H. Gerischer, Underpotential deposition of metals and work function differences, J. Electroanal. Chem. Interf. Electrochem. 54 (1974) 25.
[71] C. Batchelor-McAuley, J. Ellison, K. Tschulik, P.L. Hurst, R. Boldt, R.G. Compton, *In situ* nanoparticle sizing with zeptomole sensitivity, Analyst 140 (2015) 5048.
[72] K. Kanokkanchana, E.N. Saw, K. Tschulik, Nano impact electrochemistry: effects of electronic filtering on peak height, duration and area, ChemElectroChem 5 (2018) 3000.
[73] X. Jiao, C. Batchelor-McAuley, C. Lin, E. Kätelhön, N.P.Young E.E.L.Tanner, R.G. Compton, Role of nanomorphology and interfacial structure of platinum nanoparticles in catalyzing the hydrogen oxidation reaction, ACS Catal. 8 (2018) 6192.
[74] K.E. Young, C.A. Evans, K.V. Hodges, J.E. Bleacher, T.G. Graff, A review of the handheld X-ray fluorescence spectrometer as a tool for field geologic investigations on Earth and in planetary surface exploration, Appl. Geochem. 72 (2016) 77.
[75] D. Voiry, M. Chhowalla, Y. Gogotsi, N.A. Kotov, Y. Li, R.M. Penner, R.E. Schaak, P.S. Weiss, Best practices for reporting electrocatalytic performance of nanomaterials, ACS Nano 12 (2018) 9635.
[76] R. Sanchis-Gual, A.S.-D. Silva, M. Coronado-Puchau, T.F. Otero, G. Abellán, E. Coronado, Improving the onset potential and Tafel slope determination of earth-abundant water oxidation electrocatalysts, Electrochim. Acta 388 (2021) 138613.
[77] J.E.T. Andersen, G. Bech-Nielsen, P. Møller, J.C. Reeve, Bulk copper electrodeposition on gold imaged by *in situ* STM: morphology and influence of tip potential, J. Am. Chem. Soc. 26 (1996) 161.
[78] K. Tschulik, C. Batchelor-McAuley, H.S. Toh, E.J. Stuart, R.G. Compton, Electrochemical studies of silver nanoparticles: a guide for experimentalists and a perspective, Phys. Chem. Chem. Phys. 16 (2014) 616.
[79] T. Hachiya, H. Honbo, K. Itaya, Detailed underpotential deposition of copper on gold (III) in aqueous solutions, J. Electroanal. Chem. Interf. Electrchem. 315 (1991) 275.
[80] R.J. Randler, D.M. Kolb, B.M. Ocko, I.K. Robinson, Electrochemical copper deposition on Au (100): a combined *in situ* STM and *in situ* surface X-ray diffraction study, Surf. Sci. 447 (2000) 187.
[81] K.O. Thiel, M. Hintze, A. Vollmer, C. Donner, A new approach on the Cu UPD on Ag surfaces, J. Electroanal. Chem. 621 (2008) 7.
[82] R.E. Bolz, CRC Handbook of Tables for Applied Engineering Science, CRC Press, 2019.
[83] J. Liu, Y. Liang, T. Lui, D. Li, X. Yang, Anti-EGFR-conjugated hollow gold nanospheres enhance radiocytotoxic targeting of cervical cancer at megavoltage radiation energies, Nanoscale Res. Lett. 10 (2015) 218.
[84] Y.G. Zhou, N.V. Rees, R.G. Compton, Electrode–nanoparticle collisions: the measurement of the sticking coefficient of silver nanoparticles on a glassy carbon electrode, Chem. Phys. Lett. 514 (2011) 291.
[85] Y.G. Zhou, E.J.E. Stuart, J. Pillay, S. Vilakazi, R. Tshikhudo, N.V. Rees, R.G. Compton, Electrode-nanoparticle collisions: the measurement of the sticking coefficients of gold and nickel nanoparticles from aqueous solution onto a carbon electrode, Chem. Phys. Lett. 551 (2012) 68.
[86] T.R. Bartlett, S.V. Sokolov, R.G. Compton, Electrochemical nanoparticle sizing via nano-impacts: how large a nanoparticle can be measured? ChemistryOpen 4 (2015) 600.
[87] W. Cheng, X.F. Zhou, R.G. Compton, Electrochemical sizing of organic nanoparticles, Angew. Chem. Int. Ed. Engl. 125 (2013) 13218.
[88] W.B. Russel, Brownian motion of small particles suspended in liquids, Annu. Rev. Fluid Mech. 13 (1981) 425.
[89] W. Ma, H. Ma, J.F. Chen, Y.Y. Peng, Z.Y. Yang, H.F. Wang, Y.L. Ying, H. Tian, Y.T. Long, Tracking motion trajectories of individual nanoparticles using time-resolved current traces, Chem. Sci. 8 (2017) 1854.
[90] H. Ma, J.F. Chen, H.F. Wang, P.J. Hu, W. Ma, Y.T. Long, Exploring dynamic interactions of single nanoparticles at interfaces for surface-confined electrochemical behavior and size measurement, Nat. Commun. 11 (2020) 2307.
[91] K.Z. Brainina, L.G. Galperin, E.V. Vikulova, Electrochemistry of metal nanoparticles: the effect of substrate, J. Solid State Electrochem. 16 (2012) 2357.
[92] M. Ahmaruzzaman, A review on the utilization of fly ash, Prog. Energy Combust. Sci. 36 (2010) 327.
[93] N. Ranjbar, C. Kuenzel, Cenospheres: a review, Fuel 207 (2017) 1.
[94] A.I. Danilov, E.B. Molodkina, Y.M. Polukarov, Initial stages of copper electrocrystallization on a glassy-carbon ring–disk electrode from sulfate electrolytes of various acidity: a cyclic voltammetry study, Russ. J. Electrochem. 38 (2002) 732.
[95] I. Bimaghra, J. Crousier, Electrodeposition of copper from sulphate solutions — influence of the cations, Mater. Chem. Phys. 21 (1989) 109.
[96] K.J. V.annoy, A. Ryabykh, A.I. Chapoval, J.E. D.ick, Single enzyme electroanalysis, Analyst 146 (2021) 3413.
[97] D.S. J.ayakrishnan, Corrosion Protection and Control Using Nanomaterials, Woodhead, 2012.